Available online at www.sciencedirect.com
ScienceDirect
Catalysis Today 123 (2007) 23–30
CATALYSIS TODAY
www.elsevier.com/locate/cattod

Alkaline earth metal-based catalyst and process for selective hydrocarbon conversion to acetylene and carbon monoxide

Michael C.J. Bradford [a,*], Mure Te [b], Mahesh V. Konduru [c], Allen Pollack [d], Digna X. Fuentes [d]

[a] $|i^2|$ *Systems, P.O. Box 268, Reading, MA 01867, United States*
[b] *Saint-Gobain NorPro, 3840 Fishcreek Road, Stow, OH 44224, United States*
[c] *Johnson Matthey, 436 Devon Park Drive, Wayne, PA 19087, United States*
[d] *Lilliputian Systems, Inc., 36 Jonspin Road, Wilmington, MA 01887, United States*

Available online 14 January 2007

Abstract

A multi-step process that employs a Ni-modified mixed alkaline earth metal oxides (AEMO) has been developed for the selective conversion of hydrocarbons to C_2H_2 and CO. The initial process step is the catalytic decomposition of a gaseous hydrocarbon mixture at an elevated temperature (*ca.* 800 °C) over Ni/AEMO, generating H_2, trace CO, carbon (C), and trace alkaline earth metal carbide (MC_2). The Ni/AEMO/C/MC_2 material is then heated to consume the remaining carbon, generate more MC_2, and evolve CO. Then, Ni/AEMO/MC_2 is cooled and reacted with excess H_2O at a low temperature ($20 < T$ (°C) < 80) to selectively generate C_2H_2 and Ni/AEM$(OH)_2{\cdot}zH_2O$. In the final process step, Ni/AEM$(OH)_2{\cdot}zH_2O$ is decomposed to yield H_2O and Ni/AEMO, which is recycled within the process. The most advanced Ni/AEMO materials developed thus far exhibit intrinsic production capacities exceeding 2000 μmoles of C_2H_2 per gram of Ni/AEMO per process cycle.

Keywords: Acetylene; Natural Gas; Methane; Alkaline Earth; Carbide; Hydrolysis

1. Introduction

Many valuable chemical intermediates were once produced using C_2H_2 [1]. Currently, demand is increasing worldwide for C_2H_2 as a fuel for welding applications, and demand could grow appreciably if hurdles related to the commercialization of high-conductivity polyacetylene-based materials are overcome [2].

Approximately 68% of U.S. C_2H_2 production capacity is based on natural gas pyrolysis or partial oxidation, 18% is derived from ethylene co-production, and 14% is obtained via calcium carbide hydrolysis [1,3,4]. However, each of these technologies has distinct disadvantages. For example, arc and plasma-based routes to natural gas conversion have intrinsically high electrical costs. Pyrolysis-based processes generate dilute concentrations of C_2H_2 in the reactor effluent, thus necessitating energy-intensive and expensive downstream separation steps. Product yields are lower than the theoretical limits because intrinsic chemical kinetics and thermodynamic equilibrium generate a broad product distribution, in part because C_2H_2 can rapidly oligomerize to aromatics and decompose to coke at the elevated temperatures employed by these technologies. In addition, calcium carbide-based processes are capital and energy intensive. Consequently, there is a need for a more efficient process for selective C_2H_2 production.

Several research groups have demonstrated that C_2+ production from CH_4 can be accomplished at moderate conditions using a two-step process [5–8]. During the first process step, a supported transition metal is exposed to CH_4 at elevated temperature, during which dissociative adsorption and carbon-carbon bond formation both occur. Hydrogen is subsequently introduced in the second process step (typically at the same or a lower temperature than the first step) to hydrogenate surface carbonaceous deposits, facilitate the coupling of surface species, and stimulate product desorption. Although initial work in the area of two-step CH_4 conversion was focused on the production of C_2+ *n*-alkanes, research efforts shifted toward the production of branched alkanes,

* Corresponding author. Tel.: +1 978 203 1708; fax: +1 978 203 1799.
E-mail address: michael.bradford@i2systems.org (M.C.J. Bradford).

0920-5861/$ – see front matter © 2007 Elsevier B.V. All rights reserved.
doi:10.1016/j.cattod.2007.01.006

cycloalkanes, and olefins. Nevertheless, there are limitations to two-step CH_4 conversion:

1. The specific activity of the metal surface generates less than 5 μmol of olefins per gram of supported metal per process cycle;
2. The selectivity to C_2+ olefins during the second process step is typically less than 75%; and
3. A large quantity of excess H_2 must be used during the hydrogenation step to recover the C_2+ hydrocarbons from the metal surface.

A modified process for hydrocarbon conversion to C_2H_2 that is conceptually similar to two-step CH_4 homologation has been developed that circumvents inherent problems associated with C_2H_2 generation at elevated temperatures by dividing the process into multiple steps (Fig. 1). The overall reaction stoichiometry for the process is:

$$3CH_x + H_2O \rightarrow C_2H_2 + CO + 1.5xH_2 \quad (1)$$

The initial process step is the catalytic decomposition of a gaseous hydrocarbon mixture at elevated temperature (*ca.* 800 °C) over a Ni-modified alkaline earth metal oxide (AEMO), generating H_2, trace CO, carbon (C), and trace alkaline earth metal carbide (MC_2). The Ni/AEMO/C/MC_2 material is then heated to consume the remaining carbon, generate more MC_2, and evolve CO. Then, Ni/AEMO/MC_2 is cooled and reacted with excess H_2O at a low temperature ($20 < T$ (°C) < 80) to selectively generate C_2H_2 and Ni/AEM(OH)$_2$·zH_2O. In the final process step, Ni/AEM(OH)$_2$·zH_2O is decomposed to yield H_2O and Ni/AEMO, which is recycled within the process. Some Ni/AEMO materials and the process steps developed to use these materials to facilitate selective hydrocarbon conversion to C_2H_2 and CO are discussed herein.

2. Experimental

2.1. Material synthesis

Mixed metal carbonates ($Sr_xCa_{1-x}CO_3$) were prepared via co-precipitation. A metal precursor solution was prepared by dissolution of calcium acetate (Acros, 99% Purity) and/or strontium acetate (Alfa Aesar, 99% Purity) in deionized water. Ammonium carbonate (Acros, 99% Purity) was used as the precipitating agent, in excess, with a molarity of three times that of the metal acetate precursor solution. The cation (M^{2+}) and anion (CO_3^{2-}) solutions were then simultaneously added dropwise to a stirred beaker of deionized H_2O maintained at $7.75 \leq pH \leq 8.25$ and $65 \pm$ °C in order to precipitate $Sr_xCa_{1-x}CO_3 \cdot xH_2O$. The precipitated material was then filtered, washed repeatedly with deionized H_2O, and then dried in static air at 110 °C overnight, generating $Sr_xCa_{1-x}CO_3$.

Although thermodynamic equilibrium calculations indicate that complete decomposition of $CaCO_3$ and $SrCO_3$ in a closed system requires a temperature greater than 1100 °C, equilibrium calculations also demonstrate that complete carbonate decomposition is possible at a temperature less than 1100 °C in an open system in which there is a means to remove CO_2 from the system and therefore to maintain a low CO_2 partial pressure (this latter conclusion was verified through kinetic modeling of $CaCO_3$ decomposition and thermogravimetric analysis of $CaCO_3$ and $SrCO_3$ decomposition under a continuous N_2-purge at extremely high space velocity). Therefore, alkaline earth metal carbonate samples were heated under vacuum (530–590 mmHg) to 1100 °C at a rate of 4 °C/min, annealed at 1100 °C for 5 h, and cooled to room temperature in order to generate corresponding alkaline earth metal oxides, which were subsequently stored in sealed vials within a dessicator to minimize adsorption of atmospheric CO_2 and H_2O.

$Ni_ySr_xCa_{1-x-y}O_\delta$ samples were prepared in an analogous manner using nickel nitrate hexahydrate (Aldrich, ACS Reagent), with the exception that potassium carbonate (ACROS Organics, ACS Reagent) was used as the precipitating agent.

2.2. Material characterization

Materials were characterized using several techniques:

- Direct current plasma emission spectroscopy (DCPES) was performed with a Beckman Spectrospan VI Emission Spectrometer (Luvak Co. Inc.) to quantify material composition;

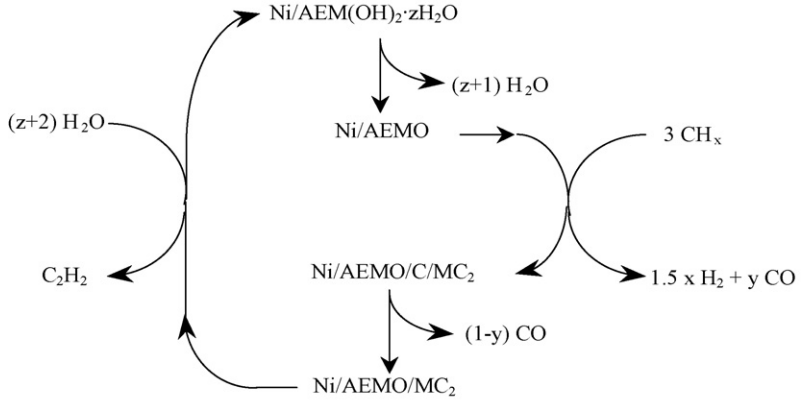

Fig. 1. A schematic process for the selective production of C_2H_2 and CO from gaseous hydrocarbons (CH_x) using Ni-modified alkaline earth metal oxide (AEMO) and metal carbide (MC_2) intermediates.

- Nitrogen adsorption isotherms were obtained with a Nova 3200 (Quantachrome Corporation) to determine the surface area; and
- X-ray diffraction (XRD) was performed using filtered, Cu Kα radiation (Materials Characterization Laboratory at the Pennsylvania State University) to determine bulk crystalline structure.

2.3. Apparatus and procedures

2.3.1. Hydrocarbon conversion

High purity N_2 (99.999%), CH_4 (99.998%), natural gas (2.44% C_2H_4, 0.214% C_3H_6, 0.120% C_4H_{10}, 1.620% N_2, 0.699% CO_2 and 94.907% CH_4), and He (99.999%) were used as received without further purification and introduced independently to a tubular quartz reactor using mass flow controllers (Porter Instrument Company, Inc.). The reactor was placed within a vertical split-tube furnace (Lindberg/Blue M, model number TF554035A) equipped with a thermocouple for external temperature control and a thermocouple inserted into the catalyst bed to monitor catalyst temperature. The reactor effluent (maintained at 120 °C) was fed to the sampling valve of an on-line gas chromatograph (SRI 8610C) equipped with a capillary column and a packed column, as well as flame ionization (FID) and thermal conductivity (TCD) detectors. The FID was used for hydrocarbon analysis and the TCD was used for hydrocarbon, H_2, N_2, CO, and CO_2 analysis. The absolute rates of CH_4 and CO_2 conversion, and H_2 and CO formation, were determined with the TCD via reference to N_2. The conversion (or formation) rates of C_2H_4, C_3H_6, and C_4H_{10}, were determined with the FID via reference to CH_4. TCD and FID response values obtained during in-house calibration were used in conjunction with those available in the literature [9].

Typically, *ca.* 2 g of ground catalyst was packed into the quartz reactor between plugs of quartz wool, and thereafter purged for 30 min at 20 °C in flowing N_2 or He. Then, the catalyst was heated under flowing N_2 or He to 827 °C at 10 °C/min, and purged for an additional 60 min. Thereafter, the diluent flow was terminated and either CH_4 or natural gas flow was introduced (GHSV = 30 to 450 $cm^3/h\ g_{cat}$). The reaction was monitored via on-line GC and terminated when the desired level of carbon accumulation had occurred (as determined via an integral mass balance), i.e., until a molar ratio of carbon to alkaline earth metal of 1/1 to 3/1 was achieved.

2.3.2. Carbide synthesis

Carbide synthesis was carried out in a dense Al_2O_3 tube (1″ OD, 36″ length, Vesuvius McDanel) under flowing high purity Ar (99.999%), which was used as received without further purification and fed to the synthesis reactor using a mass flow controller (Porter Instrument Company, Inc.). The tube was placed within a horizontal tube furnace (Lindberg/Blue M, Model STF55433C-1) equipped with a thermocouple for external temperature control. The furnace tube effluent, which was maintained at room temperature, was directly fed to the sampling valve of an on-line gas chromatograph (SRI 86010A) equipped with a packed column and a thermal conductivity detector (TCD). The rate of CO formation was calculated via reference to Ar through use of published thermal response values [9]. The amount of carbon removed from the sample during the carbide synthesis step was estimated from the rate of CO formation during each experiment via the integration of the rate of CO formation versus time spectrum (no other gaseous hydrocarbons were observed during carbide synthesis; see Section 3.2.2 for additional details). In a typical experiment, *ca.* 3–5 g of the spent material (post exposure to methane or natural gas at 827 °C) was placed upstream of a bed of Al_2O_3 fiber in the Al_2O_3 tube, purged under flowing Ar (25 sccm) for 30 min at room temperature, heated at 2.5 °C/min from 20 °C to the desired synthesis temperature (1230, 1280, 1330, 1380, or 1430 °C), maintained at the reaction temperature for up to 72 h, and then cooled to room temperature at 2.5 °C/min. Samples were then transferred under an Ar blanket to a N_2-purged glove box to avoid exposure to atmospheric H_2O and CO_2.

2.3.3. Hydrolysis

After carbide synthesis, small portions of samples were removed for examination via hydrolysis in two custom-made ''bombs'' (incorporating a 5/8″ stainless steel tube equipped with a pressure gauge, a safety-relief valve, and an injection port), the internal volumes of which were calibrated after construction. In the ''N_2 bomb,'' high purity N_2 (99.999%) was used (as received without further purification) so that the hydrocarbon product distribution could be determined via GC-FID. In the ''CH_4 bomb,'' high purity CH_4 (99.999%) was used (as received without further purification) as an inert diluent and internal standard to facilitate the quantification of C_2H_2 production (also via GC-FID). The temperature of each bomb during hydrolysis was *ca.* 25 °C and was monitored via a thermocouple attached to the outside shell of the bomb. Typically, *ca.* 20–200 mg of sample was loaded into the bomb inside of the N_2-purged glove box. Then, the bomb was removed from the glove box, pressure tested at 60 psig, and purged five times by filling the bomb with 60 psig of CH_4 or N_2 followed by evacuation for five minutes. After the last purge cycle, the bomb was pressurized with CH_4 or N_2 (to 3 psig), and 3.6 g of deionized water was injected into the bomb via the injection port. The bomb was then vigorously shaken for one minute, and the temperature and pressure of the bomb were monitored thereafter as a function of time. Gas phase samples were periodically withdrawn from the injection port and manually injected into a gas chromatograph (SRI 8610A) equipped with a 6′ × 1/8″ HayeSep S 100/120 column and a flame ionization detector (FID). The quantity of C_2H_2 in the gas-phase (μmol C as $C_2H_2/g_{material}$) was quantified via reference to CH_4 based on the temperature, pressure, and the volume of the hydrolysis unit (corrected for the volume of liquid H_2O present). The quantity of C_2H_2 dissolved in the H_2O was calculated from the measured partial pressure of C_2H_2 in the bomb through the use of its known Henry's constant (0.041 mol C_2H_2/kg_{H2O}·bar) [10].

2.3.4. Material regeneration

Regeneration of processed materials was carried out in a quartz tube (1″ OD, 24″ Length) using dilute O_2 (9.80% in He). The tube was placed within a horizontal split-tube furnace (Lindberg/Blue M, Model STF55035A) equipped with a thermocouple in the center of the heating zone for temperature measurement and control. The temperature of the tube effluent was maintained at *ca.* 25 °C. Typically, 2–3 g of the sample was packed in a quartz tube between two plugs of quartz wool, purged under flowing O_2 (50 sccm) for 60 min at 25 °C, heated at 10 °C/min to 1000 °C, maintained at 1000 °C for 10 h, and cooled to room temperature. Recovered samples were either stored in a dessicator or subjected to another cycle of hydrocarbon conversion.

3. Results

3.1. $Sr_xCa_{1-x}O$

3.1.1. Material characterization

Analytical material compositions determined via DCPES are in excellent agreement with nominal values (Table 1). Nitrogen adsorption measurements indicate that sample surface area after vacuum annealing decreases with increasing Sr content.

XRD spectra of the prepared $Sr_xCa_{1-x}O$ materials reveal the presence of cubic CaO (PDF# 37-1497), cubic SrO (PDF# 48-1477), cubic $Sr_xCa_{1-x}O$, hexagonal $Ca(OH)_2$ (PDF# 4-733), and orthorhombic $Sr(OH)_2$ (PDF# 27-874). Hydroxide phases were likely formed during collection of the XRD spectra due to sample exposure to humid air. Volume-weighted crystallite sizes (d_v) of some cubic oxide phases were calculated through application of the Scherrer Equation with Warren's correction for line broadening to the (2 0 0) reflections (Table 1).

The simultaneous presence of bulk CaO and $Sr_xCa_{1-x}O$ phases indicates a heterogeneous Sr distribution, and implies a Sr content in the $Sr_xCa_{1-x}O$ phase above that of the bulk material composition. Lattice parameters for each (*h k l*) reflection of the prepared $Sr_xCa_{1-x}O$ materials (a_{hkl}) were calculated, plotted as a function of $\cos^2\theta$, and extrapolated to $\cos^2\theta = 0$ in order to estimate a lattice parameter (a_0) for each material (Fig. 2). Calculated lattice parameters for synthesized $Sr_xCa_{1-x}O$ materials are slightly larger than values reported by the International Centre for Diffraction Data for $Sr_xCa_{1-x}O$ solid solutions (PDF #'s 48-1468 to 48-1476), indicating that the Sr contents of the prepared $Sr_xCa_{1-x}O$ phases are indeed slightly higher than the bulk strontium sample compositions.

Table 1
Composition, surface areas, and volume-weighted crystallite sizes (d_v) of $Sr_xCa_{1-x}O$ materials prepared via vacuum annealing of $Sr_xCa_{1-x}CO_3$ samples at 1100 °C

Composition (x)		Surface area (m^2/g)[b]	d_v (nm)[c]		
Nominal	Analytical[a]		CaO	$Sr_xCa_{1-x}O$	SrO
0.000	0.000	10.9 ± 1.7	43.1	–	–
0.100	0.116	5.8 ± 1.4	26.7	–	–
0.250	0.252	3.2 ± 0.9	–	8.1	–
0.500	0.496	3.1 ± 0.4	–	20.2	–
0.750	0.744	2.1 ± 0.9	–	32.0	–
1.000	1.000	1.9 ± 0.3	–	–	28.6

[a] Analytical values were measured via DCPES at Luvak Co. Inc.
[b] All reported surface areas were determined with a Nova 3200 (Quantachrome Corporation) using a 7-pt BET method and are based on the measurement of at least two independent samples ($\pm 1\sigma_{n-1}$).
[c] All values were calculated from (2 0 0) reflections in XRD spectra via the Scherrer Equation using Warren's correction for instrumental line broadening.

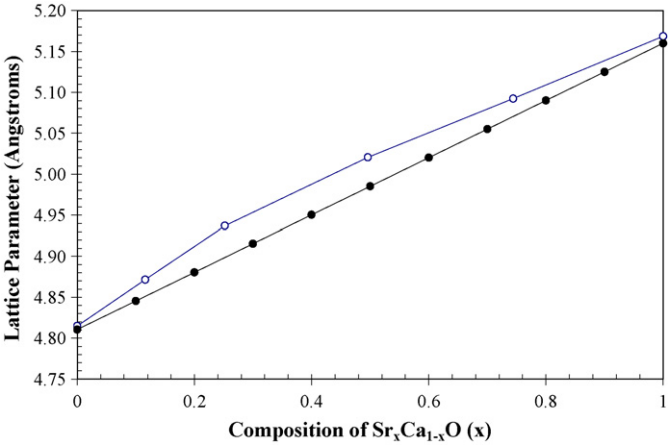

Fig. 2. A comparison of calculated lattice parameters for (○) prepared $Sr_xCa_{1-x}O$ materials with (●) values reported by the International Centre for Diffraction Data (PDF #'s 48-1468 to 48-1476).

3.1.2. Hydrocarbon conversion

The objectives of these experiments were to elucidate the role of Sr content on catalyst performance for CH_4 conversion and C_2H_2 production, in order to identify a preferred composition for additional development. The thermal pyrolysis of CH_4 was first investigated prior to the study of hydrocarbon conversion over $Sr_xCa_{1-x}O$. Results demonstrated that the rate of CH_4 conversion to coke, H_2, and higher hydrocarbons over a packed bed of quartz wool (in the absence of $Sr_xCa_{1-x}O$) was negligible at $T < 827$ °C. Therefore, this temperature was used to investigate the reactivity of CH_4 with $Sr_xCa_{1-x}O$. Inspection of the experimental results (Table 2) indicates that:

Table 2
$Sr_xCa_{1-x}O$ performance for CH_4 conversion at 827 °C (GHSV = 30 $cm^3/h\ g_{cat}$)

x	CH_4 Conversion (%)	Areal rate (μmol $CH_4/h\ m^2$)	Selectivity (%)[a]		
			Non-detected carbon	C_2+	CO_x
0.000	7.1	8.5	78.1	21.6	0.3
0.116	4.5	9.9	60.8	36.1	3.1
0.252	3.6	14.8	48.3	46.8	5.0
0.496	2.3	9.3	76.4	16.4	7.2
0.744	2.2	13.9	62.9	28.5	8.6
1.000	2.6	17.3	61.1	32.7	6.2

[a] Selectivity to non-detected carbon, gas-phase hydrocarbons (C_2+), and CO/CO_2 (CO_x) is on a carbon atom basis.

Table 3
Acetylene production during hydrolysis of $Sr_xCa_{1-x}O$ at 25 °C after exposure to CH_4 at 827 °C

x	nmol C_2H_2/g $Sr_xCa_{1-x}O$/C
0.000	0
0.116	0
0.252	0
0.496	272
0.744	13
1.000	0

- Although the rate of CH_4 conversion on a specific activity (mass) basis was highest for CaO, the rate of CH_4 conversion over Sr-containing materials was always higher on an areal basis (μmol CH_4/h m^2); and
- The selectivity for non-detected carbon (primarily in the form of coke that accumulated on the $Sr_xCa_{1-x}O$ material during reaction) was highest for CaO and $Sr_{0.5}Ca_{0.5}O$.

3.1.3. Hydrolysis

After $Sr_xCa_{1-x}O$ exposure to CH_4 at 827 °C, each material was cooled to room temperature and hydrolyzed. Inspection of the hydrolysis data reveals that the maximum C_2H_2 yield was observed for $Sr_{0.5}Ca_{0.5}O$ (Table 3). No additional data were obtained to elucidate the potential reason(s) for the exhibited differences in catalytic behavior as a function of composition. Nevertheless, based on these results, $Sr_{0.5}Ca_{0.5}O$ was selected for further development.

3.2. $Ni_ySr_xCa_{1-x-y}O_\delta$

3.2.1. Hydrocarbon conversion

The primary objectives of these experiments were to determine the influences of (1) process cycling, (2) carbide synthesis temperature, and (3) post-hydrolysis oxidation, on $Ni_ySr_xCa_{1-x-y}O_\delta$ performance for natural gas conversion to coke and H_2. Results indicate that $Ni_{0.12}Sr_{0.44}Ca_{0.44}O_\delta$ performance does not significantly change from one process cycle to the next if an oxidation step is included after material hydrolysis (Table 4).

3.2.2. Carbide synthesis

After $Ni_{0.12}Sr_{0.44}Ca_{0.44}O_\delta$ was used for hydrocarbon conversion it was subjected to carbide synthesis, during which the extent of reaction was monitored through on-line gas chromatography by measuring the rate of CO formation, presumed to form as a result of alkaline earth metal oxide reduction and carbide formation:

$$3C_{(s)} + Sr_xCa_{1-x}O_{(s)} \leftrightarrow Sr_xCa_{1-x}C_{2(s)} + CO_{(g)} \quad (2)$$

A typical plot of CO evolution as a function of time and temperature is shown in Fig. 3.

During the temperature ramp for all carbide synthesis experiments an apparent maximum rate of CO formation was observed at 763 ± 52 °C ($\pm 1\sigma_{n-1}$), a temperature range proximate to the melting points of strontium (777 °C) and

Table 4
The performance of $Ni_{0.12}Sr_{0.44}Ca_{0.44}O_\delta$ for natural gas conversion as a function of process cycling, carbide synthesis temperature, and combustion after hydrolysis[a]

$T_{carbide}$ (°C)	Reagent oxidation prior to gas conversion?	Cycle #	Natural gas conversion (%)					(C/(Sr + Ca))[b]	S_{NDC}[c] (%)	Carbon[d] accumulation (μmol C/s g_{cat})
			CH_4	C_2H_6	C_3H_8	C_4H_{10}	CO_2			
1230	Yes	1	75.5	100	100	100	100	1.14	98.4	4.30 ± 0.11
	Yes	2	67.8	100	100	100	100	–	98.4	3.90 ± 0.08
	Yes	3	73.9	100	100	100	100	–	98.2	4.20 ± 0.10
1280	Yes	1	79.5	99.8	100	100	100	0.91	68.1	3.12 ± 0.03
	Yes	2	60.3	100	100	100	100	–	97.8	3.49 ± 0.26
	Yes	3	81.5	100	100	100	100	–	98.2	4.60 ± 0.09
1330	Yes	1	82.1	100	100	100	100	1.10	98.4	4.65 ± 0.35
	No	2	10.6	98.2	100	100	100	–	91.1	0.75 ± 0.15
	No	3	9.8	97.8	100	100	100	–	91.0	0.81 ± 0.21
1380	Yes	1	85.8	100	100	100	100	1.13	98.5	4.85 ± 0.06
	No	2	7.2	94.4	100	100	100	–	77.7	0.58 ± 0.16
	No	3	8.5	96.2	100	100	100	–	83.7	0.68 ± 0.15
1430	Yes	1	76.4	98.4	100	100	100	3.35	98.2	4.34 ± 0.32
	Yes	2	68.6	100	100	100	100	–	98.0	3.93 ± 0.50
	Yes	3	69.5	100	100	100	100	–	97.7	3.97 ± 0.34

Process steps (natural gas conversion, carbide synthesis, hydrolysis and oxidation) correspond to those shown in Fig. 1. Reaction conditions: $T \approx 827$ °C; $P \approx 1$ atm; GHSV ≈ 450 cm^3/h g_{cat}; inlet natural gas composition = 2.44% C_2H_6, 0.214% C_3H_8, 0.120% C_4H_{10}, 1.620% N_2, 0.699% CO_2 and 94.907% CH_4.

[a] Reported uncertainties are non-biased standard deviations ($\pm 1\sigma_{n-1}$) and are indicative of the observed variance from the mean as a function of time-on-stream.

[b] The molar ratio of carbon deposited to alkaline earth metal (Ca + Sr) present in the material is only valid for the first process cycle, as post-mortem characterization of calcined reagents revealed the loss of both calcium and strontium during processing (see Table 6). Amounts of carbon deposition during subsequent process steps (gram carbon per gram of reagent) were of the same magnitude as the first process step for each series of data.

[c] The selectivity to non-detected carbon (S_{NDC}) is reported on a carbon atom basis.

[d] Average rates of carbon accumulation on the reagent were calculated based on an overall material balance using rates of consumption and formation measured *in situ* using on-line gas chromatography (GC). The key assumption in this calculation was that all carbon not detected in the reactor effluent by GC was deposited on the material.

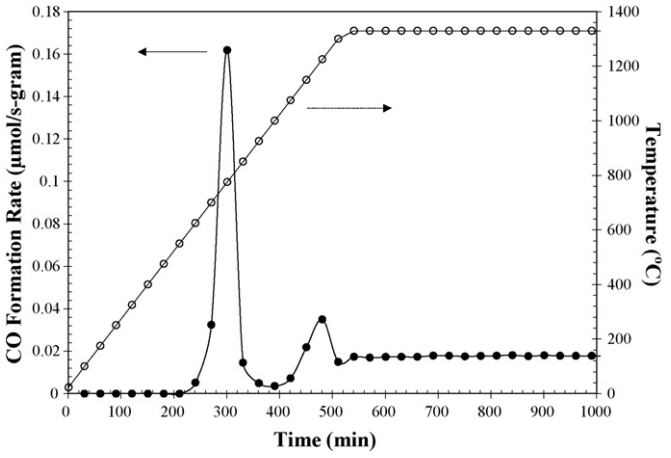

Fig. 3. The observed rate of CO formation as a function of time and temperature during carbide synthesis (e.g., $T_{carbide}$ = 1330 °C corresponds to the steady-state synthesis temperature).

calcium (842 °C), but below that used to deposit carbon (*ca.* 827 °C). Upon a further increase in temperature to the desired carbide synthesis temperature ($T_{carbide}$), another maximum in CO formation rate was typically observed, followed by a slow, declining rate throughout the remainder of the experiment. Presumably, these observations are consistent with the existence of at least three types of reactive carbon species on the material surface subsequent to natural gas decomposition. Although several types of carbon species, including filamentous carbon, are known to form on supported Ni catalysts upon exposure to hydrocarbons [14], the carbonaceous species formed on $Ni_{0.12}Sr_{0.44}Ca_{0.44}O_{\delta}$ during hydrocarbon conversion were not characterized.

3.2.3. Hydrolysis

Upon completion of carbide synthesis, samples were recovered and transferred to a dessicator in a N_2-purged glove box to minimize exposure to atmospheric moisture. Thereafter, small portions of these samples were subjected to hydrolysis at room temperature in order to generate C_2H_2, as well as quantify C_2H_2 production, selectivity, and yield (Table 5). Inspection of the data reveals that:

1. C_2H_2 production (μmol C as $C_2H_2/g_{material}$) during the initial process cycle increases with increasing carbide synthesis temperature;
2. Selectivity to C_2H_2 during the initial process cycle decreases with increasing carbide synthesis temperature;
3. C_2H_2 production decreases during subsequent process cycles for $T_{carbide} \geq 1280$ °C;
4. The extent of material deactivation (as indicated by the decrease in C_2H_2 production) increases as $T_{carbide}$ increases; and
5. C_2H_2 production yields approaching the theoretical maximum (0.88) were observed.

3.2.4. Material characterization

The composition and surface areas of calcined $Ni_ySr_xCa_{1-x-y}O_{\delta}$ as-prepared and after three complete process cycles as a function of carbide synthesis temperature ($T_{carbide}$) are provided in Table 6. The material surface area after completion of three process cycles is higher than observed for the as-prepared material (Table 1), independent of carbide synthesis temperature, indicating that cyclic reduction and re-oxidation of $Ni_ySr_xCa_{1-x-y}O_{\delta}$ induces particle attrition. In addition, elemental analysis of ''spent'' samples reveals that the Sr and Ca contents of each material decreased during cyclic testing, and that the extent of element depletion increased with increasing carbide synthesis temperature. It is interesting to note that while $Sr_xCa_{1-x-y}O$ materials for

Table 5
Acetylene production during hydrolysis of $Ni_ySr_xCa_{1-x-y}C_zO_{\delta}$ after carbide synthesis as a function of carbide synthesis temperature and process cycling

$T_{carbide}$ (°C)	Cycle #	C_2H_2 Production[a]		C_2H_2 Yield[c] (mol C_2H_2/mol $Ni_{0.12}Sr_{0.44}Ca_{0.44}C_{1.76}$)
		μmol C as $C_2H_2/g_{material}$	S (%)[b]	
1230	1	2,825 ± 235	99.96 ± 0.04	0.30
	2	3,926 ± 419	99.88 ± 0.13	0.44
	3	2,701 ± 127	99.99 ± 0.00	0.29
1280	1	4,378 ± 187	99.9 ± 0.2	0.57
	2	3,960 ± 74	99.88 ± 0.07	0.46
	3	3,122 ± 77	99.96 ± 0.00	0.32
1330	1	5,229 ± 307	97.8 ± 1.2	0.57
	2	4,920 ± 102	99.98 ± 0.01	0.41
	3	3,134 ± 204	99.19 ± 0.04	0.27
1380	1	8,262 ± 109	97.2 ± 0.6	0.88
	2	7,463 ± 268	99.93 ± 0.05	0.56
	3	2,090 ± 670	99.9 ± 0.1	0.18
1430	1	10,234 ± 232	96.0 ± 4.7	0.46
	2	6,175 ± 208	99.94 ± 0.04	0.27
	3	115 ± 61	88.4 ± 6.5	0.01

Nominal $H_2O/Ni_{0.12}Sr_{0.44}Ca_{0.44}(OH)_2$ = 83 (molar).
[a] Uncertainties are non-biased standard deviations ($\pm 1\sigma_{n-1}$) and are based on two or more measurements.
[b] Selectivity to acetylene is reported on a carbon atom basis.
[c] Acetylene yields are calculated from the observed acetylene production through use of the theoretical maximum acetylene production, as calculated from the carbon-to-alkaline earth metal atomic ratio and the *initial* reagent composition. The maximum theoretical yield is 0.88 mol C_2H_2/mol $Ni_{0.12}Sr_{0.44}Ca_{0.44}C_{1.76}$.

Table 6
Composition and surface areas of calcined $Ni_ySr_xCa_{1-x-y}O_{\delta}$ as-prepared, and after three complete process cycles as a function of carbide synthesis temperature ($T_{carbide}$)

$T_{carbide}$ (°C)	Composition (wt%)[a]			$Ni_ySr_xCa_{1-x-y}O_{\delta}$[a]			Surface area (m^2/g)[b]
	Ni	Sr	Ca	y	x	$1-x-y$	
As-Prepared[c]	8.62	48.80	22.30	0.12	0.44	0.44	1.6 ± 0.5
1280	12.60	16.00	22.50	0.22	0.19	0.59	2.8 ± 0.2
1330	14.40	4.89	29.20	0.24	0.05	0.71	2.7 ± 0.1
1380	23.10	2.91	19.40	0.43	0.04	0.53	2.5 ± 0.3
1430	50.00	3.29	4.69	0.85	0.04	0.11	4.7 ± 0.5

[a] Values were measured via DCPES.
[b] Surface areas were determined using a 7-pt BET method. Uncertainties ($\pm 1\sigma_{n-1}$) are based on the measurement of at least two independent samples.
[c] The data in this row refer to the as-prepared sample.

Table 7
Experimental lattice parameters (a_0) and volume-weighted crystallite sizes (d_v) for phases present in the XRD spectra of calcined $Ni_ySr_xCa_{1-x-y}O_\delta$ samples as-prepared and after three complete reaction cycles, compared with values previously reported for $Sr_xCa_{1-x}O$ solid solutions (Fig. 2), and values in the literature

Material	$T_{carbide}$ (°C)	a_0 (Å)[a]				d_v (nm)[b]			
		NiO	$Sr_xCa_{1-x}O$	CaO	CaC_2	NiO	$Sr_xCa_{1-x}O$	CaO	CaC_2
NiO[c]	–	4.177	–	–	–	–	–	–	–
$Sr_{0.5}Ca_{0.5}O$	–	–	5.021	–	–	–	20.2	–	–
$Ni_{0.12}Sr_{0.44}Ca_{0.44}O_\delta$	–	4.183	5.004	–	–	61.8	24.0	–	–
$Ni_{0.22}Sr_{0.19}Ca_{0.59}O_\delta$	1280	4.190	4.860	–	–	45.6	43.5	–	–
$Ni_{0.24}Sr_{0.05}Ca_{0.71}O_\delta$	1330	4.194	–	4.815	–	38.5	–	41.6	–
$Ni_{0.43}Sr_{0.04}Ca_{0.53}O_\delta$	1380	–	–	–	$a_0 = 3.817$ $c_0 = 6.598$	–	–	–	–
CaO[c]	–	–	–	4.815	–	–	–	43.1	–
CaC_2[c]	–	–	–	–	$a_0 = 3.887$ $c_0 = 6.375$	–	–	–	47.0

[a] Lattice parameters for each (h k l) reflection (a_{hkl}) were calculated for cubic unit cells, plotted as a function of $\cos^2\theta$, and extrapolated to $\cos^2\theta = 0$ in order to estimate a lattice parameter (a_0). This procedure corrects for errors due to sample absorption and the use of flat specimens [20].
[b] All d_v values were calculated via the Scherrer Equation using Warren's correction for instrumental line broadening.
[c] Reference [21].

which Sr/Ca < 1 exhibited no detectable C_2H_2 production after hydrocarbon conversion and hydrolysis (Table 3), all $Ni_ySr_xCa_{1-x-y}O_\delta$ materials exhibited Sr/Ca < 1 after cyclic testing (Table 6) and nevertheless exhibited significant C_2H_2 production (Table 5).

Although this difference is likely in large part attributable to the difference in maximum temperatures to which $Sr_xCa_{1-x-y}O$ (827 °C) and $Ni_ySr_xCa_{1-x-y}O$ (1230–1430 °C) were subjected prior to hydrolysis, it might also reflect a difference in the interactions between Sr and Ca upon Ni addition.

XRD spectra of the calcined $Ni_ySr_xCa_{1-x-y}O_\delta$ samples as-prepared and after three complete reaction cycles were analyzed to identify bulk crystalline phases and to calculate lattice parameters and volume-weighted crystallite sizes (Table 7). The spectrum for the as-prepared material is consistent with a mixture of $Sr_{0.5}Ca_{0.5}O$ and NiO (no K-containing phases were present in the XRD spectra, indicating that if K is present in the $Ni_ySr_xCa_{1-x-y}O_\delta$ samples after preparation, it's concentration is relatively low). However, after completion of three reaction cycles at $T_{carbide}$ = 1280 °C or 1330 °C, diffraction peaks for the alkaline earth metal oxide solid solution are shifted toward the positions expected for CaO, indicating the loss of Sr. In addition, the XRD spectrum of the material after multiple cycles at 1380 °C indicates the possible presence of a *tetragonal* CaC_2 phase that had formed during carbide synthesis but was somehow protected from reaction during the subsequent hydrolysis and combustion steps.

4. Discussion

The reaction of alkaline earth metal oxides with hydrocarbons in a high-temperature rotating-arc reactor to yield carbides that upon hydrolysis selectively yield C_2H_2 or C_3H_4 has been previously reported [11–13]. However, the process described herein is different, in that (a) Ni-modified, mixed alkaline earth metal oxides are used, and (b) individual process steps are used to yield H_2, CO and C_2H_2, such that in principle, high selectivity to each molecule is possible without the need for significant investment in additional separation and or purification technology.

The first process step is the catalytic decomposition of the hydrocarbon gas on the $Ni_ySr_xCa_{1-x-y}O_\delta$ surface to primarily yield H_2 and carbon:

$$3CH_{x(g)} \rightarrow 3C_{(s)} + 1.5xH_{2(g)} \quad (3)$$

As part of this process, the reduction of NiO occurs, yielding carbon oxides, H_2 and Ni, the surface of which is highly active for light hydrocarbon dissociation [14]. In addition, partial reduction of $Sr_xCa_{1-x-y}O_\delta$ to yield $Sr_xCa_{1-x-y}C_{2\delta}$ also occurs, presumably in a similar manner to the reduction of MoO_3 by CH_4 [15], as evidenced by the production of C_2H_2 during hydrolysis after exposure to CH_4 (Table 3). The amount of carbon deposited during this step should be less than the theoretical maximum for the selective production of CO and C_2H_2 during subsequent steps, i.e., $C/(Sr + Ca) \leq 3$ — see equation (2). However, experimental results obtained during development of this process indicate that $C/(Sr + Ca) \approx 1$ results in higher overall process carbon utilization efficiency.

The second step in the process generates alkaline earth metal carbide and CO:

$$3C_{(s)} + Sr_xCa_{1-x}O_{(s)} \rightarrow Sr_xCa_{1-x}C_{2(s)} + CO_{(g)} \quad (4)$$

The observed evolution of CO during experiments reported herein is consistent with the existence of up to three types of reactive carbon species on the material surface subsequent to natural gas decomposition, as is often observed on the surface of Group VIII metals after dissociative methane adsorption [8].

The carbide synthesis reaction likely proceeds in two steps [16,17]:

$$C_{(s)} + MO_{(s)} \rightarrow M + CO_{(g)} \quad (5)$$

$$2C_{(s)} + M \rightarrow MC_{2(s)} \quad (6)$$

where the physical state of M (in this study primarily Sr and Ca, although the potential participation of trace K due to the use of K_2CO_3 for material synthesis cannot be excluded at this time) is

Table 8
Acetylene production during the hydrolysis of $Ni_ySr_xCa_{1-x-y}C_wO_\delta$ after carbide synthesis at 1200–1430 °C as a function of H_2O employed (z)

z	Experimental C_2H_2 production		C_2H_2 Yield (mol C_2H_2/mol $Ni_{0.12}Sr_{0.44}Ca_{0.44}C_{1.76}$)
	μmol C as $C_2H_2/g_{material}$	S (%)	
6	7,552 ± 112	94.8 ± 0.3	0.33
42	7,638 ± 110	99.62 ± 0.02	0.34
83	8,894 ± 204	98.27 ± 0.07	0.39

Basis: $Ni_{0.12}Sr_{0.44}Ca_{0.44}(OH)_2{\cdot}zH_2O$.

determined by the physical properties of M, kinetics, and gas-liquid-solid equilibrium:

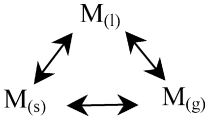

Consequently, the observed loss of Sr and Ca from the $Ni_ySr_xCa_{1-x-y}O_\delta$ materials during cyclic operation (see Table 6) is likely due (at least in part) to the volatilization of these elements during reaction at elevated temperature, followed by the transport of these elements out of the reaction zone.

The third process step, hydrolysis, selectively yields C_2H_2:

$$Sr_xCa_{1-x}C_{2(s)} + (z+2)H_2O_{(l)} \rightarrow C_2H_{2(g)} + Sr_xCa_{1-x}(OH)_2{\cdot}zH_2O_{(s)} \quad (7)$$

In the experiments reported herein, excess H_2O was typically used ($z = 83$), in accords with commercial processes for CaC_2 hydrolysis. However, more advanced hydrolysis technology uses significantly less H_2O [18–19]; therefore, the influence of excess H_2O on C_2H_2 production during hydrolysis for a sample that was subjected to carbide synthesis at 1200–1430 °C was investigated. The results illustrate that the use of H_2O in excess of that required to generate $Ni_{0.12}Sr_{0.44}Ca_{0.44}(OH)_2$-$6H_2O$ may result in improved selectivity to acetylene, and slightly higher acetylene production (Table 8).

The overall process developed and reported herein, as represented by the following stoichiometry:

$$3CH_x + H_2O \rightarrow C_2H_2 + CO + 1.5xH_2 \quad (1)$$

can be viewed as a ''deconvoluted'' catalytic cycle (Fig. 1), in which a Group VIII metal-modified alkaline earth (and possibly alkali) mixed metal oxide is the catalyst. In this regard, considering the similarity between reaction (1) and the oxidative coupling of CH_4 to $C_2H_2/C_2H_4/C_2H_6$ in the context of the experimental evidence presented herein, it seems possible that the mechanism for the oxidative coupling of CH_4 could involve the formation and subsequent reaction of carbide-like MC_2 intermediates on the catalyst surface. Unfortunately, the experimental examination of this hypothesis was beyond the scope of this investigation.

5. Summary

A multi-step process that employs Ni/AEMO materials has been developed for the selective conversion of hydrocarbons to C_2H_2 and CO. The initial process step is the catalytic decomposition of a gaseous hydrocarbon mixture at elevated temperature over Ni/AEMO, generating H_2, trace CO, carbon (C), and trace alkaline earth metal carbide (MC_2). The Ni/AEMO/C/MC_2 material is then heated to consume the remaining carbon, generate more MC_2, and evolve CO. Then, Ni/AEMO/MC_2 is cooled and reacted with excess H_2O at a low temperature ($20 < T(°C) < 80$) to selectively generate C_2H_2 and Ni/AEM$(OH)_2{\cdot}zH_2O$. In the final process step, Ni/AEM$(OH)_2{\cdot}zH_2O$ is decomposed to yield H_2O and Ni/AEMO. The overall process can be viewed as a ''deconvoluted'' catalytic cycle, in which a Group VIII metal-modified alkaline earth (and possibly alkali) mixed metal oxide is the catalyst.

Acknowledgements

This work was funded by the U.S. Department of Energy under SBIR Grant No. DE-FG02-01ER83161. The authors thank CeraMem Corporation for the release of this information to $|i^2|$ Systems.

References

[1] L.R. Roberts, in: J.J. McKetta, W.A. Cunningham (Eds.), Encyclopedia of Chemical Processing and Design, Marcel Dekker, New York, 1976.
[2] Process Economic Program Report 164: Polyacetylene. SRI Consulting, 2001.
[3] The Innovation Group: http://www.the-innovation-group.com/welcome.htm.
[4] S. Yao, A. Nakayama, E. Suzuki, Catal. Today 71 (2001) 291.
[5] M. Belgued, P. Paréja, A. Amariglio, H. Amariglio, Nature 352 (1991) 789.
[6] T. Koerts, R.A. van Santen, J. Chem. Soc., Chem. Commun. 1281 (1991).
[7] M.C.J. Bradford, Catal. Lett. 66 (2000) 113.
[8] M.C.J. Bradford, J. Catal. 189 (2000) 238.
[9] W.A. Dietz, J. Gas Chromatogr. (1967) 68.
[10] NIST (http://webbook.nist.gov/chemistry).
[11] C.S. Kim, R.F. Baddour, J.B. Howard, H.P. Meissner, Ind. Eng. Chem. Process Des. Dev. 18 (2) (1979) 323.
[12] W.A. Peters, J.B. Howard, US Patent 5,246,550 (1993); to Massachusetts Institute of Technology.
[13] W.A. Peters, J.B. Howard, US Patent 4,921,685 (1990); to Massachusetts Institute of Technology.
[14] M.C.J. Bradford, M.A. Vannice, Appl. Catal. A: Gen. 142 (1996) 73.
[15] M.C.J. Bradford, M. Te, M. Konduru, D.X. Fuentes, Appl. Catal. A: Gen. 266 (2004) 55.
[16] H. Tagawa, H. Sugawara, J. Chem. Soc. Jpn. 35 (8) (1962) 1276.
[17] J. Wang, K. Morishita, T. Takarada, Energy Fuels 15 (2001) 1145.
[18] J.W. Bunger, H. Ryu, P.A.V. Devineni, US Patent 5,284,630 (1994); to The University of Utah.
[19] J.W. Bunger, C.P. Russell, J.W. Wiser, J.C. Tsai, US Patent 6,294,148 (2001); to James W. Bunger & Associates, Inc.
[20] B.D. Cullity, Elements of X-Ray Diffraction, second ed., Addison-Wesley, Reading, 1978.
[21] CRC Handbook of Chemistry and Physics, 76th ed., CRC Press, Boca Raton, 1995.